Engineering 11 (2022) 80–86

Contents lists available at ScienceDirect

Engineering

journal homepage: www.elsevier.com/locate/eng

Research
Green Chemical Engineering—Article

Efficient Splitting of *Trans*-/*Cis*-Olefins Using an Anion-Pillared Ultramicroporous Metal–Organic Framework with Guest-Adaptive Pore Channels

Zhaoqiang Zhang [a], Xili Cui [a], Xiaoming Jiang [b], Qi Ding [a], Jiyu Cui [a], Yuanbin Zhang [a], Youssef Belmabkhout [c], Karim Adil [c], Mohamed Eddaoudi [c], Huabin Xing [a,*]

[a] *Key Laboratory of Biomass Chemical Engineering of Ministry of Education, College of Chemical and Biological Engineering, Zhejiang University, Hangzhou 310027, China*
[b] *State Key Laboratory of Structural Chemistry, Fujian Institute of Research on the Structure of Matter, Chinese Academy of Sciences, Fuzhou 350002, China*
[c] *Advanced Membranes and Porous Materials Center, King Abdullah University of Science and Technology, Thuwal 23955, Saudi Arabia*

ARTICLE INFO

Article history:
Received 30 April 2021
Revised 13 September 2021
Accepted 21 October 2021
Available online 8 December 2021

Keywords:
Adsorption and separation
Trans-/*cis*-butene
Ultramicroporous metal–organic frameworks
Pore engineering
Guest-adaptive

ABSTRACT

Trans-/*cis*-olefin isomers play a vital role in the petrochemical industry. The paucity of energy-efficient technologies for their splitting is mainly due to the similarities of their physicochemical properties. Herein, two new tailor-made anion-pillared ultramicroporous metal–organic frameworks (MOFs), ZU-36-Ni and ZU-36-Fe (GeFSIX-3-Ni and GeFSIX-3-Fe) are reported for the first time for the efficient *trans*-/*cis*-2-butene (*trans*-/*cis*-C_4H_8) mixture splitting by enhanced molecular exclusion. Notably, ZU-36-Ni unexpectedly exhibited smart guest-adaptive pore channels for trapping *trans*-C_4H_8 with a remarkable adsorption capacity (2.45 mmol·g^{-1}) while effectively rejecting *cis*-C_4H_8 with a high purity of 99.99%. The dispersion-corrected density functional theory (DFT-D) calculation suggested that the guest-adaptive behavior of ZU-36-Ni in response to *trans*-C_4H_8 is derived from the organic linker rotation and the optimal pore dimensions, which not only improve the favorable adsorption/diffusion of *trans*-C_4H_8 with optimal host–guest interactions, but also enhance the size-exclusion of *cis*-C_4H_8. This work opens a new avenue for pore engineering in advanced smart or adaptive porous materials for specific applications involving guest molecular recognition.

1. Introduction

Trans-/cis-isomers differ only in the spatial arrangement of the atoms. Remarkably, such a minor variation imparts significant differences in their reactivity in organic synthesis and pharmacological activity. *Trans*-/*cis*-olefins have important applications in chemical research and processing. For example, *trans*- and *cis*-2-butenes (C_4H_8), the simplest olefins displaying trans-/cis-isomerism, are the basic raw materials for producing various types of polymers and organic chemicals. Notably, *cis*-C_4H_8 is a crucial feedstock for the production of maleic acid, butadiene, and polymers. However, the inevitable presence of *trans*-C_4H_8 as an impurity in *cis*-C_4H_8 adversely impacts the quality of the products [1–4]. High-purity *trans*-C_4H_8 (> 95%) is significant for several applications, such as the production of propylene via the metathesis of *trans*-C_4H_8 and ethylene [5,6]. Therefore, it is highly necessary to separate *cis*-C_4H_8 and *trans*-C_4H_8. The similarity in the molecular structures and boiling points (Fig. 1(a) and Table S1 in Appendix A) of *trans*-/*cis*-olefin isomers poses great challenges in their separation [7–10]. Furthermore, 2-C_4H_8 is highly reactive and tends to undergo copolymerization or dimerization at elevated temperatures. This characteristic renders the isolation of the high purity individual 2-C_4H_8 isomers highly challenging via the traditional energy-intensive extractive distillation [9,11–12]. Size-selective physisorption using ultramicroporous materials is a promising energy-efficient alternative and has been demonstrated as a promising candidate for the efficient separation of light hydrocarbon mixtures [13–16]. However, to the best of our knowledge, the efficient separation of *trans*-/*cis*-olefin isomers by porous materials has rarely been reported.

Metal–organic frameworks (MOFs) or porous coordination polymers (PCPs) are custom-tailored porous crystalline materials with tunable pore chemistry. This kind of material has recently been successfully used as systems for separating mixtures of varying degrees of complexity [16], such as paraffins and olefins

* Corresponding author.
E-mail address: xinghb@zju.edu.cn (H. Xing).

https://doi.org/10.1016/j.eng.2021.10.013

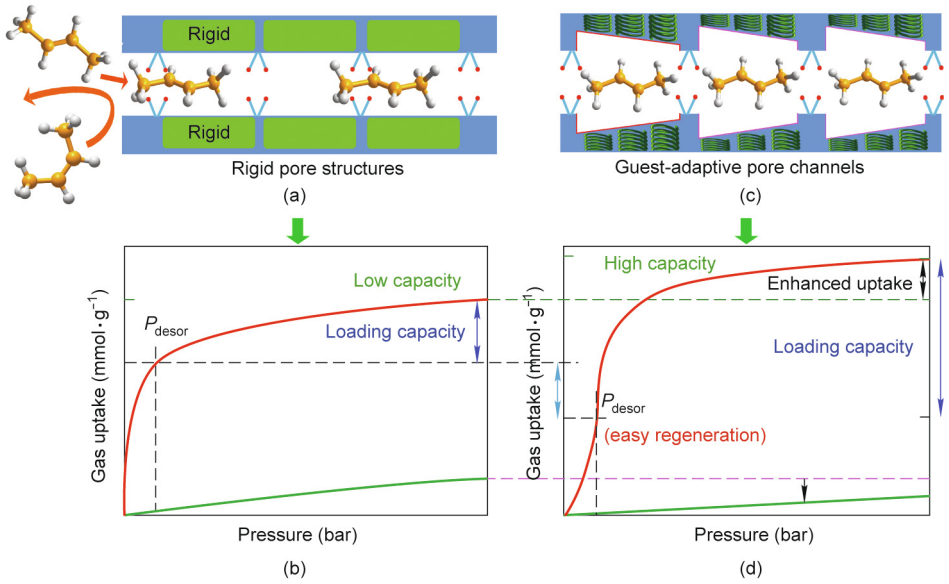

Fig. 1. Schematic of representative robust porous materials with (a) rigid pore structures and (b) a typical Langmuir adsorption isotherm for microporous materials. Novel porous materials with (c) guest-adaptive pore channels and (d) corresponding desired stepped adsorption isotherm for increasing the working capacity. 1 bar = 10^5 Pa.

[13,17–21], olefins and alkynes [23–31], n-isomer and iso-isomer mixtures [12,32–34], and other analogous molecules. However, achieving high efficiency for the high-level separation complexity using MOFs is still exceedingly challenging [16] when the differences in size and shape between the probes, such as trans-/cis-isomers, are subtle. The trans-/cis-isomer separation selectivity, and particularly the diffusivity, achieved using the current state-of-the-art MOFs is still not suitable for use in industrial processes in comparison to distillation [9]. For example, zeolitic imidazolate framework-7 (ZIF-7) with its narrow pore window size and structural flexibility exhibits gate-opening phenomenon in response to the external stimuli of *trans*-/*cis*-C_4H_8. However, both the isomers exert the same gate-opening pressure of 2 kPa, which leads to a poor separation performance [35]. Zeolites with rigid frameworks have been used to separate *trans*-/*cis*-C_4H_8 mixtures by sieving effect, however, their *trans*-C_4H_8 uptake capacity is very low at 1.05 and 0.83 mmol·g^{-1} on ITQ-32 (ITQ stands for Instituto de Tecnología Química) [36] and deca-dodecasil 3 rhombohedral (DD3R) [37], respectively, owing to the limited space available for the gas uptake in the rigid pore structures within zeolites (Fig. 1(a)). Similar low *trans*-C_4H_8 capacity was also observed for metal-gallates (Ni, Mg, and Co) owing to their robust nature [8]. In general, robust zeolites exhibit Langmuir-type adsorption isotherms for *trans*-C_4H_8 which is the cause for their limited loading capacity (Fig. 1(b)) in swing adsorption processes driven by pressure. This, in turn, presents major bottlenecks in their practical application owing to recyclability concerns. Furthermore, porous materials with large pore sizes (> 5.0 Å, 1 Å = 10^{-10} m) usually exhibit high capacity but almost no separation selectivity for *trans*-/*cis*-C_4H_8, such as Y-fum-fcu-MOF (fum stands for fumarate; fcu stands for face-centered cubic) [10] and ZJNU-30 (ZJNU stands for Zhejiang Normal University). Thus, the discovery of a porous material with optimal pore dimensions, functionality, and energetics, that could discriminate or sieve particular *trans*-/*cis*-olefin isomers without sacrificing high gas uptake capacity, is a significantly profound challenge.

Anion-pillared ultramicroporous MOFs featuring electronegative inorganic and contracted pore surface [38–41] have unveiled outstanding separation performance for several important industrial gases such as C_2H_2/C_2H_4 [28] and C_3H_6/C_3H_8 [21]. The variable combination of inorganic anions and metal ions enables the ultrafine-tuning of the pore apertures within the 0.1–0.5 Å scale [41–46]. Herein, we report the results from the further exploration of this fluorinated ultramicroporous platform that allowed us to unveil ZU-36-Ni (GeFSIX-3-Ni, $Ni(GeF_6)(pyz)_2$, GeFSIX = GeF_6^{2-}, 3 = pyrazine = pyz), which displayed an unprecedented efficiency in trapping significant amounts of *trans*-C_4H_8 while achieving effective exclusion of the *cis*-isomers (Fig. 1(c)). Importantly, ZU-36-Ni displayed an interesting step-wise adsorption isotherm that indicates an enhanced adsorption capacity and regeneration process with less energy input. Moreover, the adaptive pore channels for separating *trans*-C_4H_8, derived from the organic linker rotation for the guest molecule, conferred an increased sorption capacity to ZU-36-Ni (2.45 mmol·g^{-1}) while the contracted pore window enhanced the *cis*-C_4H_8 exclusion effect, leading to improved *trans*-/*cis*-C_4H_8 separation selectivity (Fig. 1(d)).

2. Material and methods

2.1. Materials

Nickel(II) tetrafluoroborate hexahydrate ($Ni(BF_4)_2{\cdot}6H_2O$, 99%, J&K Scientific, China), ammonium hexafluorogermanate ($(NH_4)_2GeF_6$, 99.99%, J&K Scientific), ammonium hexafluorosilicate ($(NH_4)_2SiF_6$, 99.99%, Sigma–Aldrich, USA), iron(II) tetrafluoroborate hexahydrate ($Fe(BF_4)_2{\cdot}6H_2O$, 97%, Sigma–Aldrich), and methanol (CH_3OH, anhydrous, 99.8%, Sigma–Aldrich) were purchased and used without further purification.

Trans-2-butene (*trans*-C_4H_8, 99.9%), *cis*-2-butene (*cis*-C_4H_8, 99.9%), and helium (He, 99.99%) were purchased from Hangzhou Jingong material Co., Ltd. (China). The mixture of 1,3-butadiene/*trans*-2-butene/1-butene/*cis*-2-butene/*iso*-butene/*n*-butane/*iso*-butane (45/6.5/13/5.5/24/5/1, v/v) was purchased from Shanghai Weichuang Standard Gas Co., Ltd. (China).

2.2. Material syntheses

ZU-36-Ni (GeFSIX-3-Ni) was prepared using a literature report [41]. In a typical process, 1 mmol of $Ni(BF_4)_2{\cdot}6H_2O$ (340 mg), 1 mmol of $(NH_4)_2GeF_6$ (223 mg), and 1 g of pyrazine were dissolved in 2 mL of CH_3OH and 2 mL of H_2O, and stirred at ambient

conditions for 2 d, which yielded a blue powder. The blue powder was then heated to 140 °C at 5 °C·min^{-1} and was maintained for 24 h under vacuum to obtain the ZU-36-Ni material. SIFSIX-3-Ni was synthesized with the same method except that $(NH_4)_2GeF_6$ was substituted by $(NH_4)_2SiF_6$. For ZU-36-Fe, the synthesis procedure is the same as that for GeFSIX-3-Ni, except that $Ni(BF_4)_2$·$6H_2O$ was replaced by $Fe(BF_4)_2$·$6H_2O$.

2.3. Characterization

Powder X-ray diffraction (PXRD) was conducted at room temperature on a Bruker D8 Advance diffractometer (Bruker AXS, Germany) using Cu-Kα radiation (λ = 1.5418 Å). PXRD data treatment and the structural determination were performed using the JANA2006. FullProf.98 program was applied for the Rietveld refinements. The background was refined with a polynomial function. The thermal stability of the obtained materials was investigated via thermalgravimetric analysis (TGA, TA Instruments SDT 600, USA) under N_2 atmosphere with a flow rate of 20 mL·min^{-1}.

2.4. Gas adsorption

The sorption isotherms of C_4 hydrocarbons at low pressures up to 1 bar (1 bar = 10^5 Pa) were collected on a fully automated ASAP 2050 adsorption analyzer (Micromeritics Instruments, USA). The temperature was controlled with a water circulation bath.

2.5. Breakthrough test of C_4 isomers

The fixed-bed breakthrough tests were conducted on a self-made dynamic gas breakthrough equipment [30]. The test was conducted using a stainless-steel chromatographic column with an inner diameter of 4.6 mm and length of 50 mm. Samples of ZU-36-Ni, SIFSIX-3-Ni, and ZU-36-Fe were packed in three of the same columns which weighed 0.62, 0.64, and 0.67 g, respectively. The column packed with the sample powders was first activated with a flow of He (10 mL·min^{-1}) at 100 °C for 12 h. After the activation, a *cis*-C_4H_8/*trans*-C_4H_8 (50/50, v/v) mixture with a flow rate of 0.5 mL·min^{-1} was introduced. After the breakthrough test, the fixed-bed was regenerated under He flow (5 mL·min^{-1}) at 100 °C for 12 h. The actual separation performance of the as-synthesized material for C_4 mixtures including 1,3-butadiene, *trans*-2-butene, 1-butene, *cis*-2-butene, *iso*-butene, *n*-butane, and *iso*-butane (1,3-C_4H_6/*trans*-C_4H_8/*n*-C_4H_8/*cis*-C_4H_8/*iso*-C_4H_8/*n*-C_4H_{10}/*iso*-C_4H_{10}, 45/6.5/13/5.5/24/5/1, v/v) was further investigated with a flow rate of 0.75 mL·min^{-1}. The real-time outlet gas eluted from the fixed-bed was monitored using a gas chromatography (Micro GC-490, Agilent, USA). For studying the effect of humidity on the separation performance, the *cis*-C_4H_8/*trans*-C_4H_8 (50/50, v/v) mixture with a flow rate of 1 mL·min^{-1} was introduced into a water tank at 298 K, and the outflow gas was then flowed through a sorption column. The outlet gas from the column was monitored using a GC-2010 (Shimadzu, Japan) equipped with a flame ionization detector (FID) and a thermal conductivity detector (TCD).

A correction for the dead time was applied by He breakthrough experiments, and the He retention time (He is regarded as non-adsorbed) was applied as the dead time.

3. Results and discussion

3.1. Fine-tuned pore structure

Two ultramicroporous MOFs, ZU-36-Ni and ZU-36-Fe ($Fe(GeF_6)(pyz)_2$), were prepared by the reaction of ammonium hexafluorogermanate ($(NH_4)_2GeF_6$), pyrazine, and $Ni(BF_4)_2$ or $Fe(BF_4)_2$ in a CH_3OH and H_2O mixture, followed by heating the isolated solid at 140 °C for 24 h in vacuo (Figs. 2(a) and (b)). The refined unit cell parameters of ZU-36-Ni were a = b = 6.984 Å, and c = 7.587 Å (also termed as the pore dimension of ZU-36-Ni, Table S2 in Appendix A), which is in accordance with the three-dimensional scales of *trans*-C_4H_8 (7.4 Å × 5.35 Å × 4.16 Å) and favors the preferential binding of *trans*-C_4H_8 in the unit cells of ZU-36-Ni. In contrast, ZU-36-Fe showed a longer pore cell with c = 7.73 Å, resulting from the weak coordination affinity between Fe^{2+} and the N atoms in the organic linker. Such a different pore dimension may lead to different sorption behaviors and host–guest interaction modes in limited pore space [27]. The introduction of GeF_6^{2-} with increased Ge–F distance (1.83 Å) results in one-dimensional (1D) contracted pore channels compared with SIFSIX-3-Ni (Si–F distance: 1.67 Å). The abundant electronegative F atoms protruding into the 1D pore channels can bind the guest molecule via strong H-bonding [42–45]. The quasi-maximum pore sizes (upper limit of the pore size, Fig. S1 in Appendix A) of ZU-36-Ni and ZU-36-Fe (blue break lines in Fig. 2(c)) are 4.75 and 4.85 Å, respectively. Such ultra-micro pores could efficiently exclude *cis*-C_4H_8 (4.94 Å, kinetic diameter), but allow the trapping of *trans*-C_4H_8 (4.31 Å, kinetic diameter) (Fig. 2(d)). The purity of the as-synthesized ZU-36-Ni and ZU-36-Fe was confirmed by comparing the PXRD patterns with the calculated patterns of ZU-36-Ni and ZU-36-Fe (Fig. S2 in Appendix A). The Brunauer–Emmett–Teller (BET) surface areas calculated by CO_2 adsorption isotherms at 273 K were 313 and 295 m^2·g^{-1} for ZU-36-Ni and ZU-36-Fe, respectively (Fig. S3 in Appendix A). Thermostability is a key metric that reflects certain aspects of the framework stability. The TGA results demonstrated that ZU-36-Ni is stable up to 340 °C (Fig. S4 in Appendix A), which is relatively superior to the other reported ultramicroporous MOFs such as NbOFFIVE-1-Ni (310 °C) [43] and SIFSIX-3-Ni (210 °C). The improved thermal stability of ZU-36-Ni compared with the analogous MOFs may be attributed to the short and strong bonds between Ni^{2+} and the organic linkers, and the strong binding affinity of GeF_6^{2-} with Ni^{2+}, which leads to the contracted framework. Furthermore, the structure and adsorption performance of both the anion-pillared MOFs could be well retained after exposure to humid air, indicating their high tolerance to humid air (Figs. S2 and S3).

3.2. Adsorption performances

When used as sorbents for the separation of *trans*-/*cis*-C_4H_8, ZU-36-Fe exhibited a typical Langmuir-type adsorption isotherm for *trans*-C_4H_8 with strong binding affinity and high uptake at low pressures. The *trans*-C_4H_8 uptake amount on ZU-36-Fe is 1.81 mmol·g^{-1} at 1 bar and 298 K. On the other hand, ZU-36-Ni (Fig. 3(a)) exhibited a stepped-adsorption isotherm for *trans*-C_4H_8. At the low-pressure range (< 0.01 bar), the less steep slope of the adsorption isotherm indicated that *trans*-C_4H_8 interacts less strongly with ZU-36-Ni, which caused the low capture uptake of *trans*-C_4H_8 at such low pressures. With the pressure increasing, the slope increased, indicating that ZU-36-Ni shows increased and homogeneous binding affinity for *trans*-C_4H_8. Finally, ZU-36-Ni showed a remarkable *trans*-C_4H_8 capacity of 2.45 mmol·g^{-1} (equals to one molecule per cell), which is significantly higher than that on ZU-36-Fe although the pore size is relatively smaller (Fig. 3(b)). Such reversal in adsorption behavior is attributed to the adaptivity of the pore structure of ZU-36-Ni, which allowed the enhanced accommodation of *trans*-C_4H_8 molecules. A desorption pressure (P_{desor}) of 0.01 bar was selected according to the purity and yield requirements of the product. The working capacity (Fig. S5 in Appendix A) of ZU-36-Ni, 2.25 mmol·g^{-1}, is much higher than that for ZU-36-Fe (0.77 mmol·g^{-1}). Notably, ZU-36-Ni exhibited much higher uptake for *trans*-C_4H_8 (2.45 mmol·g^{-1}) than other

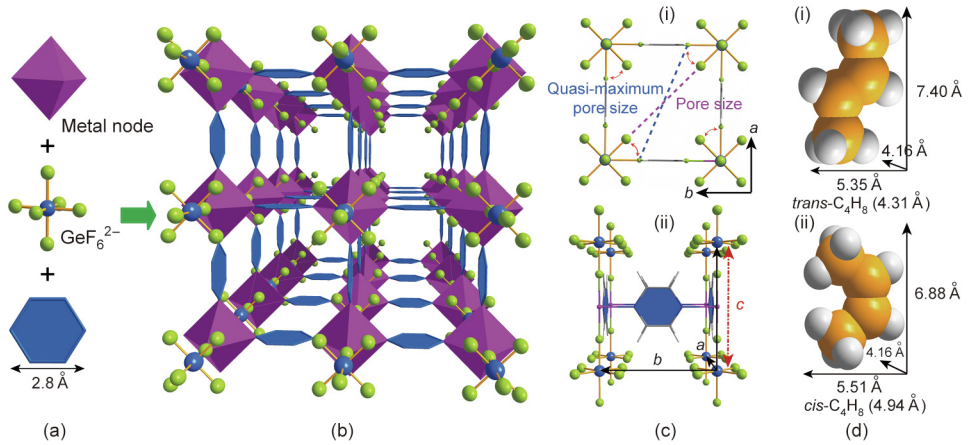

Fig. 2. Schematic illustration of (a) synthesis and (b) pore structure of ZU-36 material. (c) Quasi-maximum and empirical pore size are defined by paralleled F–F distance (blue break lines) and diagonal F–F distance (pink break lines), respectively, and the unit cell of ZU-36 viewed from *a* direction with *c* axis controlled. (d) Molecular structures and sizes of *trans*-C_4H_8 and *cis*-C_4H_8.

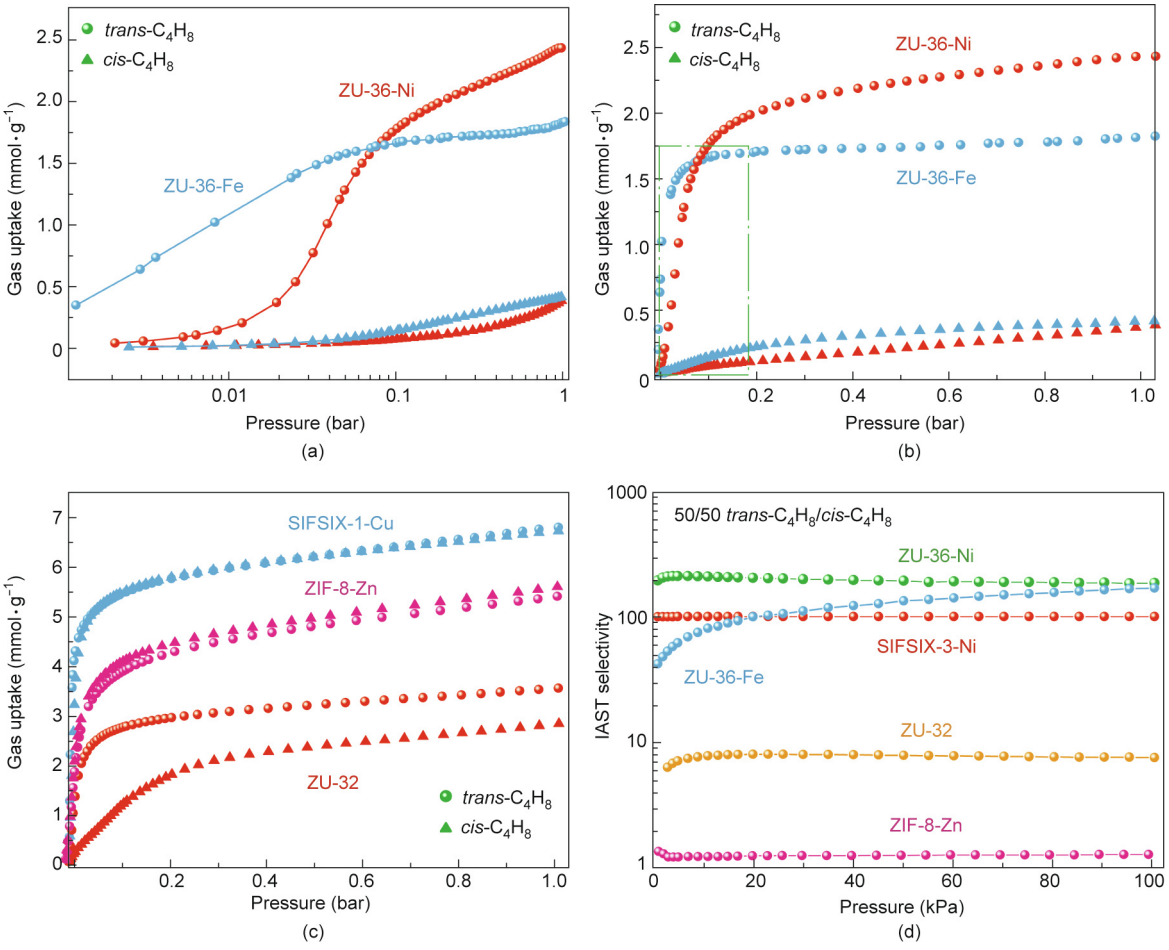

Fig. 3. (a) Stepped sorption isotherms of *trans*-C_4H_8 on ZU-36-Ni compared with (b) typical Langmuir adsorption isotherms of *trans*-C_4H_8 on ZU-36-Fe (298 K). (c) *Trans*-/*cis*-C_4H_8 adsorption isotherms on other ultramicroporous materials at 298 K. (d) Ideal adsorbed solution theory (IAST) selectivities of various MOFs for *trans*-/*cis*-C_4H_8 (50/50, v/v) mixture.

reported size-sieving materials (Table S3 in Appendix A), such as ITQ-32 (1.1 mmol·g^{-1}) [36] and DD3R [37] (0.832 mmol·g^{-1} at 303 K). In contrast, both ZU-36-Ni and ZU-36-Fe showed relatively negligible adsorption of *cis*-C_4H_8 because of the molecular exclusion effect. Owing to its relatively smaller aperture size, ZU-36-Ni (4.75 Å vs 4.85 Å for ZU-36-Fe) exhibited a lower *cis*-C_4H_8 uptake (0.35 mmol·g^{-1}) than ZU-36-Fe (0.5 mmol·g^{-1}) and SIFSIX-3-Ni (0.8 mmol·g^{-1}, Fig. S6 in Appendix A) at 1 bar and 298 K. Such a low *cis*-C_4H_8 uptake and high *trans*-C_4H_8 capacity endowed ZU-36-Ni with a benchmark *trans*-/*cis*-C_4H_8 uptake ratio

of 7, which is much higher than that of ZU-36-Fe (3.6) and the other previously reported materials such as Mg-gallate (3.2) [8], Y-fum-fcu-MOF (0.94) [10], and ZJNU-30 (1.13).

Other ultramicroporous MOFs were also investigated for comparison. Interpenetrated anion-pillared MOFs with larger pore size only exhibit moderate uptake ratios for *trans*-/*cis*-C_4H_8 (Fig. 3(c), Fig. S7 in Appendix A, and Table S3). For example, ZU-32 (GeFSIX-2-Cu-i) with a pore window size of 4.5 Å × 4.5 Å exhibits high *trans*-C_4H_8 and *cis*-C_4H_8 uptake capacity (3.55 and 2.85 mmol•g^{-1}, respectively) at 1 bar and 298 K but a low uptake ratio of 1.37 (Fig. 3(c)), and moderate separation potential. SIFSIX-1-Cu and ZIF-8-Zn exhibit high but almost the same uptake for both *trans*- and *cis*-C_4H_8, indicating the negligible separation selectivity for *trans*-/*cis*-C_4H_8 mixtures (Fig. 3(c)).

3.3. Separation selectivities

The feasible separation selectivity of anion-pillared ultramicroporous MOFs for *trans*-/*cis*-C_4H_8 (50/50, v/v) mixture were qualitatively evaluated using calculations of the ideal adsorbed solution theory (IAST) (Fig. 3(d), Table S4 in Appendix A) [47]. ZU-36-Ni and ZU-36-Fe displayed separation selectivities of 191 and 170, respectively, which were much higher than that for ZU-32 (7.6), ZIF-8-Zn (1.2), and ZJNU-30 (1.5). Furthermore, the initial slope ratios (Figs. S8–S13 and Table S5 in Appendix A) also suggest that ZU-36-Ni (18.7) exhibits excellent separation performance compared with other materials, such as Ni-gallate (7.9) [8] and ZU-32 (7), and can be a promising physical adsorbent for *trans*-/*cis*-C_4H_8 separation.

3.4. Dispersion-corrected density functional theory (DFT-D) calculations

To better understand the origin of the guest-adaptivity, the binding sites of *trans*-C_4H_8 were systematically investigated through DFT-D calculations (Figs. 4 and S14 in Appendix A). The initial ZU-36-Ni exhibited a primitive cubic (pcu) network with vicinal pyrazine rings in one cell perpendicular to each other and parallel with the inorganic pillars (Fig. 4(a)). When *trans*-C_4H_8 was trapped into the pore channels, an obvious rotation of pyrazine was observed to adapt the *trans*-C_4H_8 molecules (Figs. 4(b) and S14). *Trans*-C_4H_8 preferentially resides at the middle of the cavity because of the suitable pore dimension and π–π interactions between its sp^2 carbons and the aromatic ring of pyrazine. After saturation, one *trans*-C_4H_8 molecule is grasped by eight F atoms from the two planes with C–H···F H-bonding (distances: 2.50–2.59, 3.41, and 3.47 Å) accompanied with the pyrazine rotation by 9.5° (Fig. 4(b)), with a calculated binding energy (Δ*E*) of 49.6 kJ•mol^{-1}. Such effective binding configuration of *trans*-C_4H_8 in ZU-36-Ni results from the combination of suitable *c*-axis length (7.587 Å) and pore size of ZU-36-Ni, which affords full immobilization of one *trans*-C_4H_8 in one cell. In summary, the guest-adaptive behavior of ZU-36-Ni is realized by the rotation of organic linkers to maximize the host–guest interactions with optimal conformation. Additionally, the transport of *trans*-C_4H_8 from one cell to another in the 1D pore channels requires co-operative rotation of the pyrazines to accelerate this process owing to the limited pore space [20]. Such adaptive configuration transformation for guest molecules makes a great contribution to enhancing the recognition ability of *trans*-C_4H_8 and increasing the uptake capacity.

The calculated binding sites of *trans*-C_4H_8 in ZU-36-Fe were quite different (Fig. 4(c)). *Trans*-C_4H_8 is bound only by the four F atoms from the same plane via strong H-bonding, which indicated the availability of a large space unoccupied by the guest molecules in one unit cell. This is consistent with the adsorption isotherm of *trans*-C_4H_8 on ZU-36-Fe, and only 0.8 molecule of *trans*-C_4H_8 trapped in each unit cell of ZU-36-Fe, thus leading to a reduced uptake amount of *trans*-C_4H_8 at saturation. Such a different optimized binding configuration of *trans*-C_4H_8 in ZU-36-Fe, compared with that in ZU-36-Ni, is due to the fact that the longer *c*-axis (7.73 Å) in ZU-36-Fe could not fully match the scale or dimension of *trans*-C_4H_8. The calculated Δ*E* of *trans*-C_4H_8 on ZU-36-Fe was 60.5 kJ•mol^{-1}, which is much higher than that of ZU-36-Ni (49.6 kJ•mol^{-1}), implying the stronger host–guest interactions between *trans*-C_4H_8 with ZU-36-Fe at low *trans*-C_4H_8 loading. The lower Δ*E* on ZU-36-Ni can be ascribed to the compensation by the deformation of the framework (11.0 kJ•mol^{-1}) to adapt the guest molecule. Simultaneously, coverage-dependent adsorption enthalpy (Q_{st}) calculated based on Clausius–Clapeyron equation using the isotherms at different temperatures (Figs. S15 and S16 in Appendix A) shows that the Q_{st} for *trans*-C_4H_8 at zero loading on ZU-36-Ni is 42.0 kJ•mol^{-1} (Fig. S17 in Appendix A), which is also lower than that on ZU-36-Fe (61.8 kJ•mol^{-1}), signifying that much milder regeneration conditions are required for ZU-36-Ni compared with those for ZU-36-Fe. To confirm the easier regeneration of ZU-36-Ni, cyclic adsorption tests were conducted with the materials regenerated using the room temperature and vacuum condition (Fig. S18 in Appendix A). Indeed, the results confirmed that ZU-36-Ni can be more easily regenerated with the *trans*-C_4H_8 uptake well retained, whereas the *trans*-C_4H_8 uptake on ZU-36-Fe slightly declined under the same conditions, which may be attributed to the insufficient regeneration of ZU-36-Fe resulting from the strong binding affinity for *trans*-C_4H_8.

3.5. Breakthrough experiments

The actual separation performances of the *trans*-/*cis*-C_4H_8 (50/50, v/v) mixture on ZU-36-Ni and ZU-36-Fe were evaluated

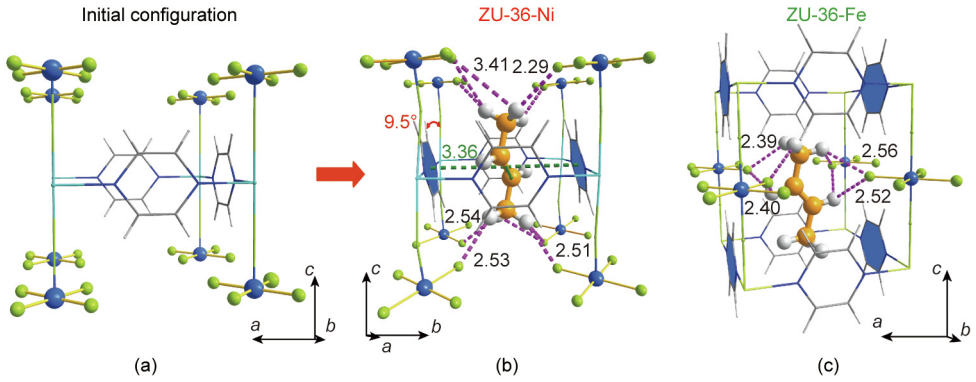

Fig. 4. (a) Initial framework of ZU-36. Binding configurations of *trans*-C_4H_8 in (b) ZU-36-Ni and (c) ZU-36-Fe, respectively, obtained by DFT-D calculations. Color code: H, gray-25%; C, gray; N, blue; Ni, turquoise; Ge, light blue; F, peak green; Fe, lime. Bond length unit: Å.

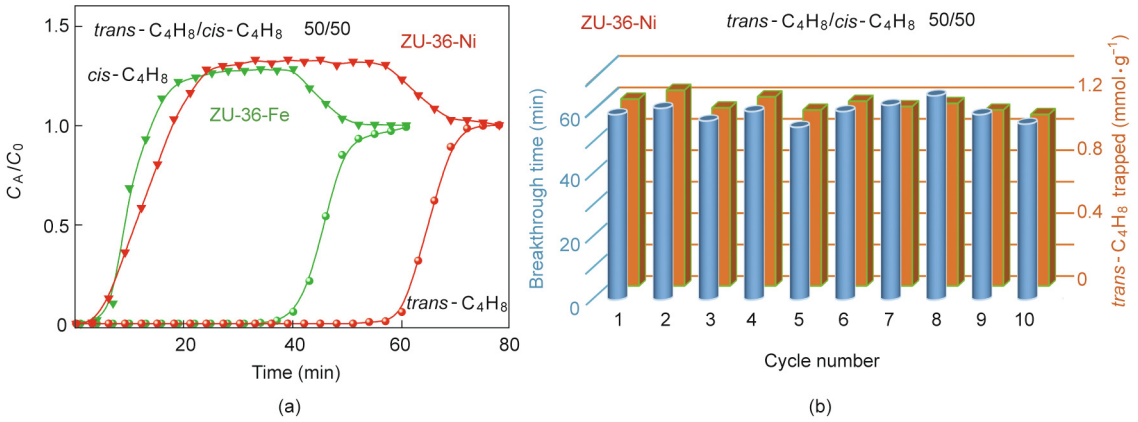

Fig. 5. (a) Breakthrough experiments for *trans*-/*cis*-C_4H_8 (50/50, v/v) mixture separation on ZU-36-Ni and ZU-36-Fe (with dead volume excluded; C_A/C_0: the relative concentration in outlet stream compared with that in feed gas). (b) Cycling breakthrough experiments for *trans*-/*cis*-C_4H_8 (50/50, v/v) separation on ZU-36-Ni.

using experimental fixed-bed breakthrough tests at 1 bar and 298 K (Fig. 5(a)). Both materials exhibit excellent *trans*-/*cis*-C_4H_8 separation performances. *Cis*-C_4H_8 elutes out of the column of ZU-36-Ni or ZU-36-Fe almost simultaneously with high purity (> 99.99%), indicating the excellent sieving effect of both materials for *cis*-C_4H_8. *Trans*-C_4H_8 could be trapped in the ZU-36-Ni fixed bed for about 58 min (93.5 min·g^{-1}) with the corresponding capture amount of 1.15 mmol·g^{-1}, which is better than that of ZU-36-Fe (37 min, 55.2 min·g^{-1}) with a capture amount of 0.72 mmol·g^{-1}. Additionally, a sharp molecular cut-off behavior for the separation of *trans*-/*cis*-C_4H_8 mixture was not observed when using SIFSIX-3-Ni (Fig. S19 in Appendix A), which is consistent with the isotherms of *trans*-/*cis*-C_4H_8 on the material (Fig. S6). More importantly, for ZU-36-Ni, there was no noticeable loss in *trans*-C_4H_8 adsorption and separation capacity even after 10 cycles of breakthrough experiments (Fig. 5(b)), illustrating the excellent structural and cycling stability of ZU-36-Ni for *trans*-/*cis*-C_4H_8 mixtures separation. Furthermore, the separation performance is unimpeded by humidity (Fig. S20 in Appendix A) showcasing the strong potential of ZU-36-Ni for *trans*-/*cis*-C_4H_8 mixture separation for industrial applications. Last but not least, ZU-36-Ni also exhibited good separation performance for the C_4 mixture (1,3-C_4H_6/*trans*-C_4H_8/*n*-C_4H_8/*cis*-C_4H_8/*iso*-C_4H_8/*n*-C_4H_{10}/*iso*-C_4H_{10}, 45/6.5/13/5.5/24/5/1, v/v, Fig. S21 in Appendix A) indicating that ZU-36-Ni is a promising material for C_4 hydrocarbon separation.

4. Conclusions

In summary, two anion-pillared ultramicroporous MOFs, ZU-36-Ni (GeFSIX-3-Ni) and ZU-36-Fe (GeFSIX-3-Fe) are reported for the first time and used for highly efficient *trans*-/*cis*-C_4H_8 splitting. ZU-36-Ni with its guest-adaptive pore channels coming from the rotation of organic linkers, exhibited an interesting step-wise adsorption isotherm for *trans*-C_4H_8. This attribute confers ZU-36-Ni with an increased capacity (2.45 mmol·g^{-1}) compared to ZU-36-Fe (1.81 mmol·g^{-1}) that does not possess adaptive pore channels. In addition, ZU-36-Ni adsorbed less *cis*-C_4H_8 than ZU-36-Fe, as ZU-36-Ni with the contracted pore window size excluded *cis*-C_4H_8 with a higher efficiency. The excellent *trans*-/*cis*-C_4H_8 separation selectivity (191) and high-purity *cis*-C_4H_8 (99.99%) observed in the breakthrough tests present ZU-36-Ni as an ideal adsorbent for *trans*-/*cis*-C_4H_8 separation. This work provides new insights into the structural property–adsorption relationships necessary for anticipating the discovery of smart and efficient porous materials for the separation of hydrocarbon isomers of different dimensions and shapes.

Acknowledgments

This work was supported by the Zhejiang Provincial Natural Science Foundation of China (LZ18B060001), and the National Natural Science Foundation of China (21725603, 21476192, and U1862110).

Compliance with ethics guidelines

Zhaoqiang Zhang, Xili Cui, Xiaoming Jiang, Qi Ding, Jiyu Cui, Yuanbin Zhang, Youssef Belmabkhout, Karim Adil, Mohamed Eddaoudi, and Huabin Xing declare that they have no conflict of interest or financial conflicts to disclose.

Appendix A. Supplementary data

Supplementary data to this article can be found online at https://doi.org/10.1016/j.eng.2021.10.013.

References

[1] Wojcieszak R, Santarelli F, Paul S, Dumeignil F, Cavani F, Gonçalves RV. Recent developments in maleic acid synthesis from bio-based chemicals. Sustain Chem Process 2015;3(1):9.
[2] Fenard Y, Dayma G, Halter F, Foucher F, Serinyel Z, Dagaut P. Experimental and modeling study of the oxidation of 1-butene and *cis*-2-butene in a jet-stirred reactor and a combustion vessel. Energy Fuels 2015;29(2):1107–18.
[3] Limsangkass W, Praserthdam P, Phatanasri S, Panpranot J, Poovarawan N, Jareewatchara W, et al. Comparative effect of nano-sized ZrO_2 and TiO_2 additional supports in silica-supported tungsten catalysts on performance in metathesis of mthylene and 2-butene to propylene. Catal Lett 2014;144(9):1524–9.
[4] Ricci G, Leone G, Boccia AC, Pierro I, Zanchin G, Mauri M, et al. Perfectly alternating ethylene/2-butene copolymers by hydrogenation of highly stereoregular 1,4-poly(1,3-diene)s: synthesis and characterization. Macromolecules 2017;50(3):754–61.
[5] Limsangkass W, Phatanasri S, Praserthdam P, Panpranot J, Jareewatchara W, Na Ayudhya SK, et al. Effect of nano-sized TiO_2 additional support in WO_3/SiO_2 catalyst systems on metathesis of ethylene and *trans*-2-butene to propylene. Catal Lett 2013;143(9):919–25.
[6] Maksasithorn S, Praserthdam P, Suriye K, Devillers M, Debecker DP. WO_3-based catalysts prepared by non-hydrolytic sol-gel for the production of propene by cross-metathesis of ethene and 2-butene. Appl Catal A Gen 2014;488:200–7.
[7] Tijsebaert B, Varszegi C, Gies H, Xiao FS, Bao X, Tatsumi T, et al. Liquid phase separation of 1-butene from 2-butenes on all-silica zeolite RUB-41. Chem Commun 2008(21):2480–2.
[8] Chen J, Wang J, Guo L, Li L, Yang Q, Zhang Z, et al. Adsorptive separation of geometric isomers of 2-butene on gallate-based metal–organic frameworks. ACS Appl Mater Interfaces 2020;12(8):9609–16.
[9] Gehre M, Guo Z, Rothenberg G, Tanase S. Sustainable separations of C_4-hydrocarbons by using microporous materials. ChemSusChem 2017;10(20):3947–63.

[10] Assen AH, Virdis T, De Moor W, Moussa A, Eddaoudi M, Baron G, et al. Kinetic separation of C_4 olefins using Y-fum-fcu-MOF with ultra-fine-tuned aperture size. Chem Eng J 2021;413:127388.
[11] Maes M, Alaerts L, Vermoortele F, Ameloot R, Couck S, Finsy V, et al. Separation of C_5-hydrocarbons on microporous materials: complementary performance of MOFs and zeolites. J Am Chem Soc 2010;132(7):2284–92.
[12] Liu H, He Y, Jiao J, Bai D, Chen DL, Krishna R, et al. A porous zirconium-based metal–organic framework with the potential for the separation of butene isomers. Chemistry 2016;22(42):14988–97.
[13] Kishida K, Okumura Y, Watanabe Y, Mukoyoshi M, Bracco S, Comotti A, et al. Recognition of 1,3-butadiene by a porous coordination polymer. Angew Chem Int Ed Engl 2016;55(44):13784–8.
[14] Liao PQ, Huang NY, Zhang WX, Zhang JP, Chen XM. Controlling guest conformation for efficient purification of butadiene. Science 2017;356 (6343):1193–6.
[15] Bao Z, Chang G, Xing H, Krishna R, Ren Q, Chen B. Potential of microporous metal–organic frameworks for separation of hydrocarbon mixtures. Energy Environ Sci 2016;9(12):3612–41.
[16] Li JR, Sculley J, Zhou HC. Metal–organic frameworks for separations. Chem Rev 2012;112(2):869–932.
[17] Zhang Z, Peh SB, Kang C, Chai K, Zhao D. Metal–organic frameworks for C_6–C_8 hydrocarbon separations. Energy Chem 2021;3(4):100057.
[18] Adil K, Belmabkhout Y, Pillai RS, Cadiau A, Bhatt PM, Assen AH, et al. Gas/vapour separation using ultra-microporous metal–organic frameworks: insights into the structure/separation relationship. Chem Soc Rev 2017;46 (11):3402–30.
[19] Zhao X, Wang Y, Li DS, Bu X, Feng P. Metal–organic frameworks for separation. Adv Mater 2018;30(37):e1705189.
[20] Ding Q, Zhang Z, Yu C, Zhang P, Wang J, Cui X, et al. Exploiting equilibrium-kinetic synergetic effect for separation of ethylene and ethane in a microporous metal–organic framework. Sci Adv 2020;6(15):eaaz4322.
[21] Lin R, Xiang S, Zhou W, Chen B. Microporous metal–organic framework materials for gas separation. Chem 2020;6(2):337–63.
[22] Fan W, Yuan S, Wang W, Feng L, Liu X, Zhang X, et al. Optimizing multivariate metal–organic frameworks for efficient C_2H_2/CO_2 separation. J Am Chem Soc 2020;142(19):8728–37.
[23] Bloch ED, Queen WL, Krishna R, Zadrozny JM, Brown CM, Long JR. Hydrocarbon separations in a metal–organic framework with open iron(II) coordination sites. Science 2012;335(6076):1606–10.
[24] Antypov D, Shkurenko A, Bhatt PM, Belmabkhout Y, Adil K, Cadiau A, et al. Differential guest location by host dynamics enhances propylene/propane separation in a metal–organic framework. Nat Commun 2020;11(1):6099.
[25] Cadiau A, Adil K, Bhatt PM, Belmabkhout Y, Eddaoudi M. A metal–organic framework-based splitter for separating propylene from propane. Science 2016;353(6295):137–40.
[26] Lee CY, Bae YS, Jeong NC, Farha OK, Sarjeant AA, Stern CL, et al. Kinetic separation of propene and propane in metal–organic frameworks: controlling diffusion rates in plate-shaped crystals via tuning of pore apertures and crystallite aspect ratios. J Am Chem Soc 2011;133(14):5228–31.
[27] Li JR, Kuppler RJ, Zhou HC. Selective gas adsorption and separation in metal–organic frameworks. Chem Soc Rev 2009;38(5):1477–504.
[28] Zhang Z, Peh SB, Wang Y, Kang C, Fan W, Zhao D. Efficient trapping of trace acetylene from ethylene in an ultramicroporous metal–organic framework: synergistic effect of high-density open metal and electronegative sites. Angew Chem Int Ed Engl 2020;59(43):18927–32.
[29] Xue DX, Belmabkhout Y, Shekhah O, Jiang H, Adil K, Cairns AJ, et al. Tunable rare earth fcu-MOF platform: access to adsorption kinetics driven gas/vapor separations via pore size contraction. J Am Chem Soc 2015;137 (15):5034–40.
[30] Yang S, Ramirez-Cuesta AJ, Newby R, Garcia-Sakai V, Manuel P, Callear SK, et al. Supramolecular binding and separation of hydrocarbons within a functionalized porous metal–organic framework. Nat Chem 2015;7(2):121–9.
[31] Zhang Z, Ding Q, Cui J, Cui X, Xing H. Fine-tuned pore dimension in hybrid ultramicroporous materials boosting simultaneous trapping of trace alkynes from alkenes. Small 2020;16(49):e2005360.
[32] Cui X, Chen K, Xing H, Yang Q, Krishna R, Bao Z, et al. Pore chemistry and size control in hybrid porous materials for acetylene capture from ethylene. Science 2016;353(6295):141–4.
[33] Wu X, Xie Y, Liu J, He T, Zhang Y, Yu J, et al. Integrating multiple adsorption sites and tortuous diffusion paths into a metal–organic framework for C_3H_4/C_3H_6 separation. J Mater Chem A 2019;7(44):25254–7.
[34] Zhang Z, Cui X, Yang L, Cui J, Bao Z, Yang Q, et al. Hexafluorogermanate (GeFSIX) anion-functionalized hybrid ultramicroporous materials for efficiently trapping acetylene from ethylene. Ind Eng Chem Res 2018;57 (21):7266–74.
[35] Zhang PD, Wu XQ, He T, Xie LH, Chen Q, Li JR. Selective adsorption and separation of C2 hydrocarbons in a "flexible-robust" metal–organic framework based on a guest-dependent gate-opening effect. Chem Commun 2020;56 (41):5520–3.
[36] Li J, Bhatt PM, Li J, Eddaoudi M, Liu Y. Recent progress on microfine design of metal–organic frameworks: structure regulation and gas sorption and separation. Adv Mater 2020;32(44):2002563.
[37] Zhang Z, Yang Q, Cui X, Yang L, Bao Z, Ren Q, et al. Sorting of C_4 olefins with interpenetrated hybrid ultramicroporous materials by combining molecular recognition and size-sieving. Angew Chem Int Ed Engl 2017;56(51):16282–7.
[38] Zhang Z, Tan B, Wang P, Cui X, Xing H. Highly efficient separation of linear and branched C_4 isomers with a tailor-made metal–organic framework. AIChE J 2020;66(7):e16236.
[39] Sholl DS, Lively RP. Seven chemical separations to change the world. Nature 2016;532(7600):435–7. Corrected in: Nature 2016;533(7601):316.
[40] van den Bergh J, Gücüyener C, Pidko EA, Hensen EJM, Gascon J, Kapteijn F. Understanding the anomalous alkane selectivity of ZIF-7 in the separation of light alkane/alkene mixtures. Chemistry 2011;17(32):8832–40.
[41] Palomino M, Cantín A, Corma A, Leiva S, Rey F, Valencia S. Pure silica ITQ-32 zeolite allows separation of linear olefins from paraffins. Chem Commun 2007 (12):1233–5.
[42] Zhu W, Kapteijn F, Moulijn JA, Jansen JC. Selective adsorption of unsaturated linear C_4 molecules on the all-silica DD3R. Phys Chem Chem Phys 2000;2 (8):1773–9.
[43] Subramanian S, Zaworotko MJ. Porous solids by design: $[Zn(4,4'\text{-}bpy)_2(SiF_6)]_n{\cdot}x$DMF, a single framework octahedral coordination polymer with large square channels. Angew Chem Int Ed Engl 1995;34(19):2127–9.
[44] Noro S, Kitagawa S, Kondo M, Seki K. A new, methane adsorbent, porous coordination polymer. Angew Chem Int Ed Engl 2000;39(12):2081–4.
[45] Shekhah O, Belmabkhout Y, Chen Z, Guillerm V, Cairns A, Adil K, et al. Made-to-order metal–organic frameworks for trace carbon dioxide removal and air capture. Nat Commun 2014;5(1):4228.
[46] O'Nolan D, Kumar A, Zaworotko MJ. Water vapor sorption in hybrid pillared square grid materials. J Am Chem Soc 2017;139(25):8508–13.
[47] Nugent P, Belmabkhout Y, Burd SD, Cairns AJ, Luebke R, Forrest K, et al. Porous materials with optimal adsorption thermodynamics and kinetics for CO_2 separation. Nature 2013;495(7439):80–4.
[48] Kumar A, Hua C, Madden DG, O'Nolan D, Chen KJ, Keane LJ, et al. Hybrid ultramicroporous materials (HUMs) with enhanced stability and trace carbon capture performance. Chem Commun 2017;53(44):5946–9.
[49] Zhang Z, Ding Q, Cui X, Jiang XM, Xing H. Fine-tuning and selective-binding within an anion-functionalized ultramicroporous metal–organic framework for efficient olefin/paraffin separation. ACS Appl Mater Interfaces 2020;12 (36):40229–35.
[50] Chen KJ, Scott H, Madden D, Pham T, Kumar A, Bajpai A, et al. Benchmark C_2H_2/CO_2 and CO_2/C_2H_2 separation by two closely related hybrid ultramicroporous materials. Chem 2016;1(5):753–65.
[51] Zhang Z, Ding Q, Peh SB, Zhao D, Cui J, Cui X, et al. Mechano-assisted synthesis of an ultramicroporous metal–organic framework for trace CO_2 capture. Chem Commun 2020;56(56):7726–9.
[52] Bhatt PM, Belmabkhout Y, Cadiau A, Adil K, Shekhah O, Shkurenko A, et al. A fine-tuned fluorinated MOF addresses the needs for trace CO_2 removal and air capture using physisorption. J Am Chem Soc 2016;138(29):9301–7.
[53] Walton KS, Sholl DS. Predicting multicomponent adsorption: 50 years of the ideal adsorbed solution theory. AIChE J 2015;61(9):2757–62.